Proceedings of the Institute of Acoustics

APPLICATION OF A RECIPROCITY TECHNIQUE FOR THE DETERMINATION OF THE CONTRIBUTIONS OF VARIOUS REGIONS OF A VIBRATING BODY TO THE SOUND PRESSURE AT A RECEIVER POINT.

J M Mason & F J Fahy

University of Southampton, Highfield, Southampton, England

1. INTRODUCTION

Interior noise of frequencies greater than about 400 Hz in private cars is often determined largely by airborne radiation from the vibrating surfaces of the engine and ancillary systems. It is difficult to separate airborne noise from structure-borne noise (through engine mounts, suspensions, etc.) without making expensive and time-consuming alterations to the structural connections. The principle of acoustic reciprocity offers an alternative and convenient means of separating these two components, while at the same time providing information on the relative contributions of various regions of the vibrating engine surface to the noise received at the ears of the passengers or driver.

Presented in this report are results that demonstrate that total received airborne noise may be separated into contributions from contiguous sub-areas of a baffled, point-excited vibrating panel. The use of phase-independent power measurements is considered for the case when no simple reference to the excitation phase is available.

2. LIST OF SYMBOLS

f	frequency (Hz)	r	position vector (m)
G	Green function (m - theory, $kgm^{-4}s^{-1}$ - exper.)	S	body surface (m^2)
		v	velocity (ms^{-1})
G_{ij}	cross spectrum	V	voltage (V)
H	transfer function	δS	panel surface elemental area
n	unit vector (m)	ρ	density (kg/m^3)
p	acoustic pressure (Nm^{-2})	ω	circular frequency ($=2\pi f$)
Q	volume velocity (m^3s^{-1})		

Subscripts

e	at observation point
g	at vibration generator terminals
i,j	integer variables
n	normal
p	at panel surface

Note the convention $X = \tilde{X}e^{j\omega t}$ is used for complex quantities.

3. THEORY

The sound field radiated by a vibrating solid body into a surrounding fluid is determined solely by the shape of the body and the distribution of vibrational acceleration normal to its surface. This fact is expressed mathematically by the Helmholtz-Kirchhoff integral equation

$$p(r) = \int_S \left[\frac{\partial p(r_s)}{\partial n}\right] G(r,r_s)\, dS \qquad (1)$$

where r is the observer point, r_s is a surface point, $\partial p/\partial n$ is the gradient of acoustic pressure normal to the body surface (proportional to the normal acceleration) and G is the Green function which satisfies the condition of zero normal gradient on the body surface. For bodies of complex shape, G takes complicated forms which are not easily calculable, even by modern numerical methods. However, G may be measured simply by placing a small, omni-directional source at a selected receiver point, and measuring the transfer function between acoustic pressure on the surface of the passive body and the volume velocity of the (calibrated) source (Fig.1). Equation (1) may be rewritten as

$$p(r) = -i\omega\rho_0 \sum_i (v_i \Delta S)\, G_i(r,r_s), \qquad (2)$$

since $\frac{\partial p}{\partial n} = -i\omega\rho_0 v$. Noting that $v_i \Delta S = Q_i$, surface volume velocity, reciprocity gives

$$\frac{p(r)}{Q_i} = -i\omega\rho_0\, G_i(r,r_s) = \frac{p_i}{Q(r)}.$$

Equation 2 may be rearranged to the form

$$p(r) = \sum_i (v_i \Delta S)\frac{p_i}{Q(r)}. \qquad (3)$$

In equation (3) it is seen that the method consists of approximating the surface integral of equation (1) by a summation over a set of discrete points on the body surface. The acceleration of the running engine is measured at the same set of points as the transfer functions and combined with the latter to predict the sound pressure at the receiver point. The result is valid provided that (i) the whole system behaves linearly, (ii) a sufficient density of measurement points is selected. The technique accounts for all paths between the engine surface and the receiver point, irrespective of whether they involve structural vibration or not. Clearly, it is possible to assess the relative contributions of the various regions on the engine to the received sound pressure, and to predict the effect of suppressing them.

4. EXPERIMENTATION

The technique was validated by tests in a normal laboratory on a system consisting of a five-sided, heavy box to which was clamped a 6.25 mm thick panel on the open side: this thickness is thought to be reasonably representative of typical, average block casting thicknesses. The panel had surface dimensions 48cm x 48cm, when clamped into a 5.33 cm wide frame along all edges (see fig. 2). The panel was excited by a vibration generator (a magnet and coil assembly inside the box) using band-limited random noise and the drive voltage V_g was used as a reference to the excitation. Normal velocity v_p, was measured on a grid of 81 points over the panel using an accelerometer. Sound pressure p_p was measured at the surface of the panel at the same locations as v_p. An observation point was chosen to provide a direct line of sight to the panel. A 2.54cm thick, large chipboard panel was inserted between the observation point and box to remove the direct path. An existing, calibrated omni-directional source Q_e was used in the experiments, placed so as to be acoustically coincident with the microphone p_e at the observation point.

Each experiment divided into two halves. Firstly, with panel excited by the shaker, the transfer function $\tilde{p}_e/\tilde{V}_g$ was measured, i.e. the 'referenced' pressure at the observation point. In addition, the transfer functions $(\tilde{v}_p/\tilde{V}_g)_i$ were acquired for each of the i=1 to 81 sub-areas of the panel. Secondly, with the volume velocity source at the observation point providing the excitation, the transfer functions $(\tilde{p}_p/\tilde{Q}_e)_i$ were acquired, again for each of sub-areas of the panel. From equation 3 for discrete measurements we have:

$$\frac{\tilde{p}_e}{\tilde{V}_g} = \sum_{i=1}^{81} \left[\frac{\tilde{p}_p}{\tilde{Q}_e}\right]_i \left[\frac{\tilde{Q}_p}{\tilde{V}_g}\right]_i , \qquad (4)$$

where $\tilde{Q}_p = \tilde{v}_p.\delta S$. Two experimental configurations are considered here. These are for

(i) the direct path present between the observation point and the simple panel,
(ii) the direct path blocked between the observation point and a non-uniform panel.

The non-uniform panel was identical to the uniform panel except for an aluminium slab of dimensions 16cm x 16 cm x 1.25 cm, glued to the underside (see fig. 3). Along with the direct path there existed secondary paths via nearby walls, ceiling, equipment and cupboards. These dominated when the direct path was obstructed.

5. RESULTS

The result shown in figure 4, for the first case, gives the comparison between the direct measurement and the prediction (comprising 162 transfer functions and calibration). Although discrepancies arise in a few narrow bands the agreement is generally good. Figure 5 shows the relative phase between the two, which should (of course) be zero at all frequencies. Large phase inaccuracies are only seen to occur at points of low response.

Figure 6 show the result for case (ii), and a similar degree of agreement is found. It is noted that the response is reduced, in most frequency bands, with the introduction of the screen and is improved, at lower frequencies, by the addition of the inhomogeneity.

5.1 Influence of point density.
The radiation of sound from the panel is related to transverse bending waves excited in the panel, and a coherent near field local to the point of excitation. Adequate point density is determined by the need to represent the smallest acoustic wavelength to be radiated by the panel. [Since the panel critical frequency is around 2000Hz, over most of range of analysis (400-2000Hz) the radiation efficiency will be low]. At 2000Hz, the wavelength of sound in air at 20°C is 0.17m, so the chosen measurement grid used to generate the results shown (figs 4-6) is clearly adequate to comply with the minimum requirement of half-wavelength sampling. If the data from the previous results is reprocessed using only 9 points (a 3 x 3 array, each sub-area δS had dimensions 16cm x 16cm) then it is reasonable to expect severe discrepancy between direct and predicted levels, at least down to 1050Hz, below which adequate sampling is still predicted. It was found that a favourable comparison exists below 700Hz, but above this the consequence of undersampling is apparent. Generally the phase information in the prediction is no longer correct.

5.2 Diagnostics.
Once it has been verified that the multi-pathed prediction is satisfactorily close to the direct measurement, then it is possible to perform some diagnostics tests on the data. It is simple, in the first instance, to see the effect of the removal of any one path on the result of the remaining summation, i.e. if one path is acoustically treated (and assumed to be removed, without altering anything else about the system) how will this effect the pressure level at the observer point? Figure 7 shows such an analysis for case (i) (simple panel, direct field present), in terms of changes in third octave bands. The reduction (or enhancement) of sound pressure at the observer point is indicated in grey-scale for each sub-area of the panel as it is removed from the summation (equation (2), note cell A is the best to treat, B is the worst). It is possible that the best areas indicated for treatment correpond to anti-nodal regions of panel modes, or, in the case of 397Hz third octave band, that a coherent near-field to the excitation point is seen. The improvement due to the omission of any one cell is small, due to the large number of cells and the uniformity of the panel.

It is not possible to verify these changes experimentally since they are within the limits of experimentally accuracy (= 2 to 3dB repeating the same complete experiment). A more clear cut result might be expected in the more complex geometry and non-uniformity of an actual engine block. It must be remembered that the results shown correspond to the effect of the removal of the contributions of individual squares. Before acoustically treating a larger area of adjacent black squares the analysis should be repeated for the omission of all the removed cells together.

5.3 Absence of a 'Reference'.
The drive voltage to the shaker coil, in the experiment described above, provides a very good reference since it is 'flat' in frequency terms and is completely correlated with the excitation. In the case of engine block, where the noise generated is due to a number of processes, no simple reference to the excitation exists. An alternative arbitrary reference could be adopted, such as the pressure at a point near to the engine, or a measurement scheme involving the acquisition of cross-spectra could be used. Under this scheme the transfer functions $H_i = (\tilde{p}_p/\tilde{Q}_e)_i$ are acquired as before and structure surface vibration is represented by cross spectra measurements $G_{ij} = \tilde{v}_i\tilde{v}_j^*$, then

$$\tilde{p}\tilde{p}^* = |\tilde{p}|^2 = \sum_i \sum_j H_i H_j^* G_{ij} \qquad (5)$$

It would be understandably tempting to dispose of the need for a reference to vibration and make simple estimates, viz

$$|\tilde{p}|^2 = \sum_i H_i H_i^* G_{ii}\,, \qquad (6)$$

where $G_{ii} = \tilde{v}_i\tilde{v}_i^* = |\tilde{v}|^2$, the vibration autospectra. For the case of a panel vibrating at frequencies not much below its critical frequency, this should lead to an error in the predicted sound level since the omitted cross-terms are still expected to make a definite contribution. In addition, it is reasonable at lower frequencies that a coherent near-field region around the point of excitation on the structure may dominate the observed sound pressure. In this case an underestimate may be obtained, since the enhancement due to adjacent cells vibrating in phase is neglected. The analysis suggested in equation 6 was performed on the data obtained in the above experiments, i.e.

$$\left|\frac{\tilde{p}_e}{\tilde{v}_g}\right| = \left[\sum_i \left|\frac{\tilde{p}_p}{\tilde{Q}_e}\right|_i^2 \left|\frac{\tilde{Q}_p}{\tilde{v}_g}\right|_i^2\right]^{1/2}, \qquad (7)$$

and compared with the prediction obtained by the linear analysis (equation 4). The result for test (i) is shown, in 1/3 octave bands, in figure 8. Generally, a significant underestimate is produced by the approximation of equation 7.

If the sound pressure level at the observation point is determined simply by a forced panel response local to the point of excitation, then it is possible to obtain an accurate prediction using only contributions from the local sub-areas, neglecting the rest of the panel. The summation in equation 4 has been repeated for 28 'local' squares (cf figure 7) and the vibrational 'near-field' prediction is compared with the direct and whole-panel prediction results in figure 9, once again in third octave bands. At low frequencies the observed pressure is dominated by the near-field since the 'near-field' prediction is seen to be roughly equal to the direct measurement. At higher frequencies, the near field progressively shrinks and other parts of the panel contribute more efficiently as the critical frequency is approached. The near-field prediction tends towards an underestimate of 6dB since only a third of the panel data has been used.

6. CONCLUSIONS

It has been demonstrated that the sound pressure at an observation point may be obtained by summing the contributions of contiguous sub-areas from a baffled, point-excited vibrating panel, with reasonable accuracy. It follows that the relative contributions of the sub-areas of the panel to the sound pressure at the observation point may be determined. In principle, insight into the efficient application of acoustic treatment to the radiating surface may be obtained from the acquired data. Along with the condition of system linearity it is also requirement of this technique that adequate discretisation of the radiating surface is implemented. The use of simple power estimates that neglect phase information has been shown to be flawed.

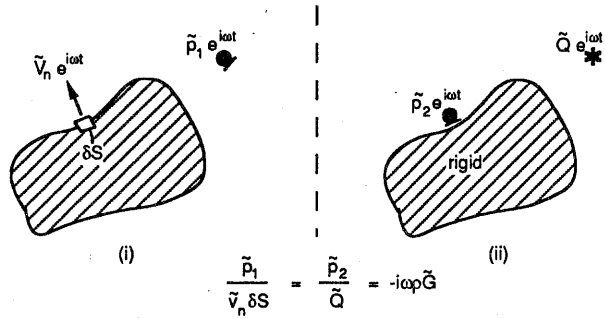

Figure 1. Reciprocal measurement of the Green function

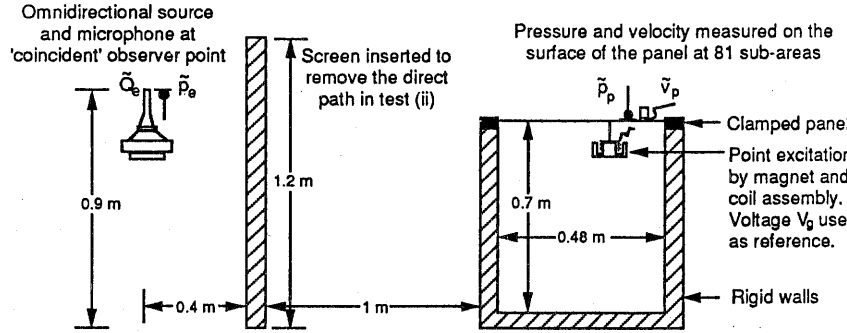

Figure 2. The test rig.

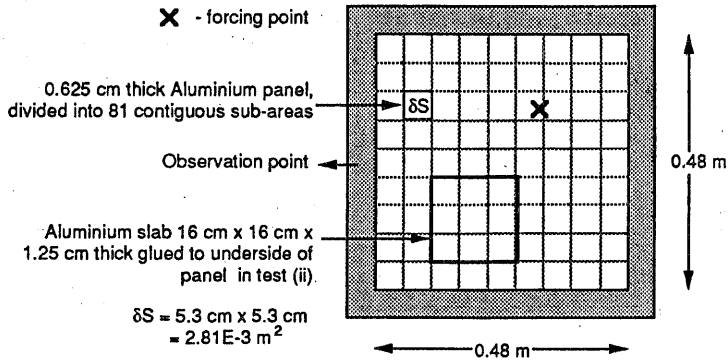

Figure 3. Description of panels used in the tests

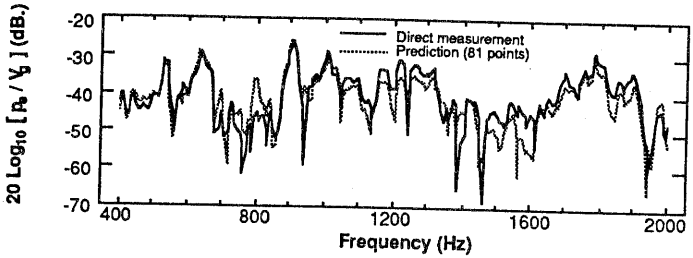

Figure 4. Comparison of direct and predicted pressure magnitude at the observation point for test (i) (simple panel, direct path present).

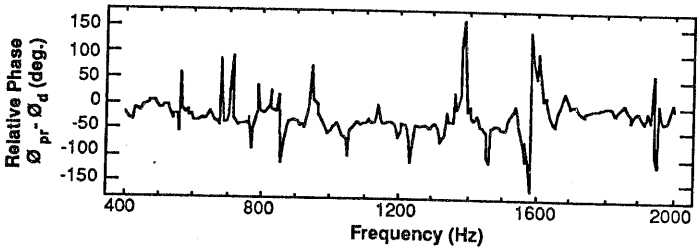

Figure 5. Relative phase between direct and predicted pressure at the observation point for test (i) (simple panel, direct path present).

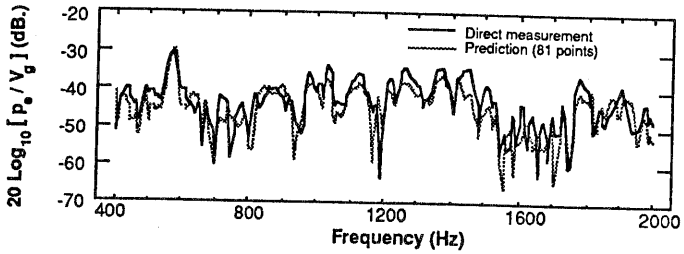

Figure 6. Comparison of direct and predicted pressure magnitude at the observation point for test (ii) (non-uniform panel, direct path blocked).

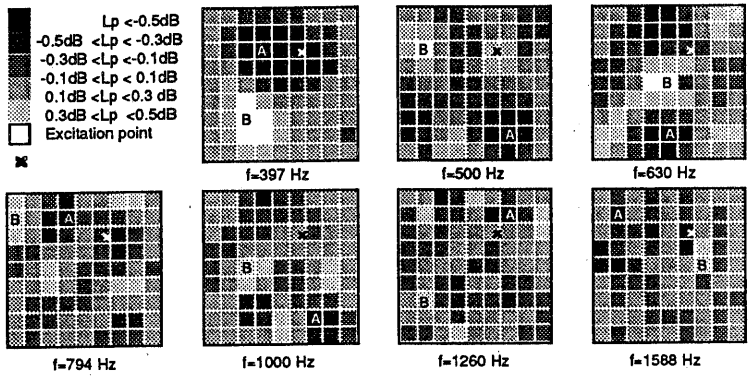

Figure 7. Schematic of the effect of removing the contribution of individual sub-areas of the panel to the observation point pressure, for test (i) (simple panel, direct path present). Note: black squares are the best to treat.

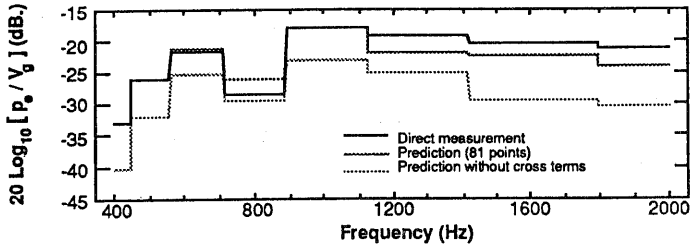

Figure 8. Comparison of direct, predicted and 'simple estimate excluding cross-terms' pressure magnitude in 1/3 octave bands at the observation point for test (i) (simple panel, direct path present).

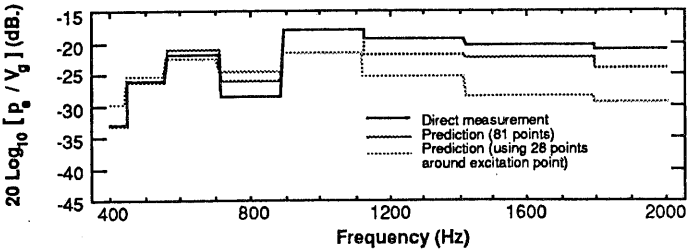

Figure 9. Comparison of direct, predicted and 'excitation near field estimate' pressure magnitude in 1/3 octave bands at the observation point for test (i) (simple panel, direct path present).